Icarus 302 (2018) 134–144

Contents lists available at ScienceDirect

Icarus

journal homepage: www.elsevier.com/locate/icarus

Testing models for the formation of the equatorial ridge on Iapetus via crater counting

Amanda L. Damptz[a], Andrew J. Dombard[a,*], Michelle R. Kirchoff[b]

[a] Department of Earth and Environmental Sciences, University of Illinois at Chicago, 845 W. Taylor St., Chicago, IL 60607-7059, USA
[b] Southwest Research Institute, 1050 Walnut Street, Suite 300, Boulder, CO 80302, USA

ARTICLE INFO

Article history:
Received 11 April 2016
Revised 24 October 2017
Accepted 30 October 2017
Available online 11 November 2017

Keywords:
Iapetus
Satellites, surfaces
Cratering
Satellites, formation
Saturn, satellites

ABSTRACT

Iapetus's equatorial ridge, visible in global views of the moon, is unique in the Solar System. The formation of this feature is likely attributed to a key event in the evolution of Iapetus, and various models have been proposed as the source of the ridge. By surveying imagery from the Cassini and Voyager missions, this study aims to compile a database of the impact crater population on and around Iapetus's equatorial ridge, assess the relative age of the ridge from differences in cratering between on ridge and off ridge, and test the various models of ridge formation. This work presents a database that contains 7748 craters ranging from 0.83 km to 591 km in diameter. The database includes the study area in which the crater is located, the latitude and longitude of the crater, the major and minor axis lengths, and the azimuthal angle of orientation of the major axis. Analysis of crater orientation over the entire study area reveals that there is no preference for long-axis orientation, particularly in the area with the highest resolution. Comparison of the crater size-frequency distributions show that the crater distribution on the ridge appears to be depleted in craters larger than 16 km with an abruptly enhanced crater population less than 16 km in diameter up to saturation. One possible interpretation is that the ridge is a relatively younger surface with an enhanced small impactor population. Finally, the compiled results are used to examine each ridge formation hypothesis. Based on these results, a model of ridge formation via a tidally disrupted sub-satellite appears most consistent with our interpretation of a younger ridge with an enhanced small impactor population.

1. Introduction

Iapetus, Saturn's third largest moon, is the only known body in the Solar System with a mountainous equatorial ridge. The ridge extends >75% of the circumference of the satellite (though not continuously) and has been heavily modified by impacts and landslides. Detailed topographic analysis confirmed that the peaks on the ridge are variable, ranging from sharp steep peaks, flat tops (trapezoidal), or numerous parallel ridge crests (Singer et al., 2009; Singer and McKinnon, 2011; Singer et al., 2012; Lopez Garcia et al., 2014). The formation of the ridge is likely attributed to a key event in the evolution of Iapetus. Studying the ridge can yield information about the formation, evolution, and the history of Iapetus. Various models (reviewed in Section 2.1) have been proposed as the source of the ridge, all of which fall under two broad categories: endogenic or exogenic. In this study, we test these formational models by exploring the population of impact craters on the surface of Iapetus as each ridge formation model makes predictions about the expectant crater population.

Studying impact craters and their distribution is a primary tool used to learn about the geologic history of planetary bodies. If the crater population is well constrained, it can then be used to determine relative ages, absolute model ages (if the impacting projectile population is known), resurfacing rates, to provide clues about subsurface properties, and to explore the evolution of the surface and planetary body as a whole (e.g., Melosh, 1989). To date, only a few groups have published their work on the impact craters and their distribution on Iapetus (Denk et al., 2010; Hirata, 2016; Kirchoff and Schenk, 2009, 2010; Martin and Jurdy, 2010; Neukum et al., 2005, Rivera-Valentin et al., 2014; Schmedemann et al., 2008, 2009). In this study, we present a crater database that includes 7748 craters on and around Iapetus's ridge. We then use the database to investigate the qualitative and quantitative characteristics of the crater population to reconstruct the age of the ridge relative to the surrounding terrain. Finally, we delve deeper into the compiled results to examine each ridge formation hypothesis and discuss the likelihood of the ridge formation models.

* Corresponding author.
E-mail address: adombard@uic.edu (A.J. Dombard).

https://doi.org/10.1016/j.icarus.2017.10.049
0019-1035/

Table 1
Hypothesis matrix of ridge formation models.

Class	Model	Author(s)	Predictions[a]		
			Early Ridge Formation	Modified Craters	E-W Elongated Craters
Endogenic	Despinning	Porco et al. (2005)	1	1	0
		Castillo-Rogez et al. (2007)	1	1	0
		Robuchon et al. (2010)	1	1	0
	Critical Spin State	Kreslavsky and Nimmo (2010)	1	1	0
	Upwarping of Lithosphere	Giese et al. (2008)	1	0	0
		Czechowski and Leliwa-Kopystyński (2008)	1	0	0
		Roberts and Nimmo (2009)	1	1	0
	Cryovolcanism	Melosh and Nimmo (2009)	1	1	0
	Planetary Contraction	Sandwell and Schubert (2010)	1	1	0
		Beuthe (2010)	1	1	0
Exogenic	Ancient Ring System	Ip (2006)	1	0	1
	Impact Generated	Levison et al. (2011)	1	0	1
		Dombard et al. (2012)	0	0	1
		Kuchta et al. (2015)	X	0	1

[a] Yes (1), No (0), Unknown (X)

2. Methods

Our analysis involves three parts. From the existing literature, we have compiled a list of attributes for the expectant crater populations of the various models of ridge formation (Section 2.1, Table 1). Next, we describe the construction of the database of the crater population on and around the equatorial ridge (Section 2.2), followed by a description of the statistical analysis used to investigate the qualitative and quantitative characteristics of the crater population (Section 2.3).

2.1. Crater populations predicted from formation hypotheses

Published hypotheses of ridge formation can be separated into seven distinct classes: despinning, critical spin state, lithospheric upwarping, cryovolcanism, planetary contraction, an ancient ring system, and giant impact. Table 1 summarizes the testable predictions of each hypothesis as discussed below.

2.1.1. Despinning

Iapetus is currently locked in a 1:1 spin-orbit resonance with Saturn and rotates/revolves with a period of 79.33 days. A best-fit ellipsoid to Iapetus's global shape displays a 33.6 km difference between the equatorial and polar radii, which is inconsistent with the current spin rate of Iapetus (Porco et al., 2005; Castillo-Rogez et al., 2007; Thomas et al., 2007; Thomas, 2010); this oblate shape is more consistent with the equilibrium figure for a hydrostatic body rotating with a period of ~16 h (Thomas et al., 2007). It is common for satellites of the major planets to become tidally despun from an initially faster rotation (Peale, 1977; Melosh, 1977). Several groups have attributed Iapetus's flattened shape to freezing in of a rotational bulge after despinning (Porco et al., 2005; Castillo-Rogez et al., 2007; Robuchon et al., 2010), although this interpretation is equivocal (e.g., Sandwell and Schubert, 2010; Kay and Dombard, 2011). Castillo-Rogez et al. (2007) and Robuchon et al. (2010) suggested that early in Iapetus's history, short-lived radioactive isotopes provided enough heat to decrease initial bulk porosity and promote tidal dissipation. During this time, the lithosphere was thin, and the ridge formed due to the change in shape and porosity. In principle, a body should also experience a loss of its oblateness (e.g., relaxation of the equatorial bulge) during the process of despinning. For Iapetus however, the lithosphere thickened due to interior cooling and was able to freeze the bulge to reflect the ~16 h spin state (Castillo-Rogez et al., 2007).

The global tectonic pattern of a despun body should include contractional features (thrust faults) orientated perpendicular to the equator (Melosh, 1977; Pechmann and Melosh, 1979). Thus, the E-W trend of the equatorial ridge on Iapetus is inconsistent with a body that has experienced tidal despinning (Melosh, 1977; Porco et al., 2005; Dombard et al., 2012). In addition, detailed studies of lineaments (linear surface features) away from the ridge do not correlate with predicted patterns due to despinning on either hemisphere (Singer and McKinnon, 2011). However, other studies have shown that variations in lithospheric thickness can change the character of the global stress field to be consistent with the orientation of the ridge (Beuthe, 2010; Melosh and Nimmo, 2009). In any event, global stresses, even away from the equator, would have been high during despinning, and one might expect a subset of the most ancient craters on Iapetus to be overprinted with tectonic features arising from these stresses.

Despinning models place the age of the ridge early in Iapetus's history and should result in a crater age relatively close to the time of accretion. A planetary body that has undergone despinning is also expected to have complex tectonic patterns (Melosh, 1977; Pechmann and Melosh, 1979). A surface that is affected by tectonics should have modified craters; here, we define modified craters as any crater subsequently overprinted by geologic processes, e.g., tectonism, volcanism, etc. The great age suggests that crater saturation, in which surfaces reach an equilibrium point where on average new craters erase pre-existing craters, may be possible. If crater saturation is reached (a possibility for all models), relative ages could be obstructed.

2.1.2. Critical spin state

As discussed above, several groups have attributed the oblate spheroid shape of Iapetus to a higher spin rate early in its history but fail to account for why the ridge sits exactly on the equator and is only on the equator. To explain the presence of the ridge, Kreslavsky and Nimmo (2010) proposed that by the end of accretion, Iapetus reached an extremely high spin rate close to a critical rate when gravity at the equator is equal to centrifugal acceleration. A model of a small, near-critically spinning asteroid, (66391) 1999 KW_4, with a roughly similar equatorial feature was used to draw similarities between the bodies. Under this model, the material at the surface of Iapetus is expected to behave similarly to this rubble-pile asteroid (cohesionless dry friction) and resulted in the buildup of the ridge. But because Iapetus is closer to a body in hydrostatic equilibrium (i.e., self-gravity dominates over material strength in determining overall shape), this model cannot be quantitatively applied, as such bodies near a critical spin limit will tend to bifurcate into a triaxial ellipsoid (Weidenschilling, 1981). Additionally, tidal despinning would need to occur later in Iapetus's history, and the lithosphere would need to be strong enough

to support the ridge. Subsequent impacts are expected to alter the surface to explain the non-continuous nature of the ridge.

The critical spin state model places the age of the ridge early in Iapetus's history. After the critical spin state is reached, despinning is necessary to produce the current shape and spin rate. A planetary body that has undergone despinning from a near critical state is expected to have complex tectonic patterns globally that will transform the oldest craters.

2.1.3. Lithospheric upwarping

Several authors have proposed that the equatorial ridge could be the result of upwarping of the lithosphere from below (Giese et al., 2008; Czechowski and Leliwa-Kopystyński, 2008; Roberts and Nimmo, 2009). Using Cassini stereo images to study the topography of Iapetus's leading side, Giese et al. (2008) argued the morphology of the ridge suggests an endogenic origin. In this scenario because low slope measurements from profiles across the equatorial ridge are less than canonical values of the angle of repose (expected for something built from above), the appearance of the ridge is consistent with it having been formed by material rising from below due to upwarping of the lithosphere. However, because of the complexity of the particulate physics, critical slope angles of stability are variable and can be quite low (e.g., Dombard et al., 2013). Giese et al. (2008) did not specify any mechanisms that would produce upwarping of the lithosphere or why deformation would be restricted solely to the equatorial region.

Czechowski and Leliwa-Kopystyński (2008) considered the possibility that the ridge is the result of surface uplift acting above an ascending current of solid-state two-cell convection. Three different scenarios were proposed to explain the existence of the ridge: spin-orbit resonance, convection in a low viscosity interior, and impact generated flow. In the first scenario, a series of consecutive spin-orbit resonances appeared after accretion. The consecutive resonances locked the rotation rate, which extended the time of despinning, and resulted in intensive tidal heating. The tidal heating promoted convection that subsequently formed the ridge. A break in resonance occurred at some point, and Iapetus began to spin down into a lower degree resonance and convection stopped. During this stage, the ridge is in an unstable orientation with respect to the Iapetus-Saturn line. Finally, Iapetus reached its present 1:1 spin-orbit resonance and reorientation where the Iapetus-Saturn lines passes through the plane of the equatorial ridge. The second scenario considered the presence of ammonia in the interior of Iapetus. An interior that is enriched in ammonia is expected to convect without any additional heat sources. Much like the spin-orbit resonance scenario, reorientation would occur during the final stage. The final scenario posited a large impact on the surface that would induce the interior convective flow field, although the authors noted that this impact generated flow scenario is less likely to have occurred due to the lack of evidence of a large impact at one of the poles.

Roberts and Nimmo (2009) also investigated whether tidal dissipation due to early despinning would promote formation of convective upwelling. From their preliminary findings, the model produced elevated topography at the equator. However, the model was unable to generate a ridge as tall or narrow as the actual ridge found on Iapetus. Additional mechanisms, such as near-surface ice or intrusive dikes, were invoked to help produce the narrow nature of the ridge.

Based on the models proposed, upwarping of the lithosphere from below (regardless of the mechanisms) should only move the pre-existing terrain upwards; thus there should be no difference in the crater population, although surface faulting may transform ancient craters. Some scenarios in Czechowski and Leliwa-Kopystyński (2008) required True Polar Wander, which would produce a tectonic signature that could overprint older craters. The Roberts and Nimmo (2009) model required cryovolcanism that could bury pre-existing craters and give the ridge a lower crater density, although some craters could show evidence of transformation via partial cryovolcanic flooding.

2.1.4. Cryovolcanism

Melosh and Nimmo (2009) suggested the only geologic features analogous to the ridge on Iapetus are volcanic dikes forming in a tensile stress environment. The length, linearity, symmetry, and somewhat discontinuous nature of the ridge are similar to terrestrial dike exposures, although the constant strike and lack of nearby lineaments or faults are uncommon (Singer and McKinnon, 2011). Tidal despinning and convection are expected as driving forces in production of the dikes due to the difficulties in concentrating the intrusion precisely on the equator. In this model, non-uniform surface temperatures are expected to produce a thinner equatorial lithosphere. Partial melting will occur where the lithosphere is thinnest and hottest. Some amount of extrusive volcanism is also expected, as the full width of the ridge cannot be attributed to intrusive material alone.

The multi-model approach proposed by Melosh and Nimmo (2009) includes tidal despinning, convection, and cryovolcanism. The authors argued that the timing of despinning and convection could occur concurrently, thus placing the age of the ridge early in Iapetus's history. The convection would lead to a concentration of rising warm currents, and partial melting would occur at the equator. Both intrusive and extrusive cryovolcanism are expected to occur. Extrusive cryovolcanism would overprint older craters, conceivably resetting the surface and giving the ridge a lower crater density, although it is equally conceivable that partial flooding of craters will yield a large fraction of modified craters near the ridge.

2.1.5. Planetary contraction

Sandwell and Schubert (2010) proposed Iapetus's present oblate shape is the result of planetary contraction and buckling failure of the lithosphere focused at the equator. In this model, Iapetus would start in a slightly oblate shape with initial porosity $>10\%$. The exterior shell would remain porous while radioactive heating from long-lived isotopes would promote compaction of the interior ice by 10% due to loss of porosity. Buckling failure of the lithosphere would then occur to accommodate the reduced volume of the interior, although the mechanism by which any localization to the equator might occur was not specified. Compaction redistributes material to build the equatorial ridge and would have happened early in the satellite's evolution.

Beuthe (2010) attempted to predict global tectonic patterns due to contraction and despinning. It is known that despinning alone prevents the formation of the E-W trend of the equatorial ridge (Melosh, 1977; Porco et al., 2005). In this latter study, the model included a lithosphere with variable thickness to demonstrate that contraction and despinning can change the character of stresses in an elastic shell of uniform thickness. Modeling of an elastic shell thinner at the equator with despinning alone produced thrust faults striking in the E-W direction primarily at the equator. When contraction was added to despinning, the thrust faults shifted from N-S to E-W. The ridge is suggestive of a compressional event long before Iapetus despun as despinning inhibits the formation of E-W tectonics. However, the combination of the despinning and contraction is not needed if the latter is sufficient. Thus, the planetary contraction models place the age of the ridge early on in Iapetus's history with a surface that has been altered by tectonics.

2.1.6. Ancient ring system

Ip (2006) suggested the equatorial ridge system could have been produced by collisional accretion of an orbital ring subse-

quent to the formation of the proto-Iapetus, composed of remnant material from accretion. Three stages of this ring system resulted in mass accumulation on the surface of Iapetus in the equatorial region. First during Iapetus's early accretionary stage, molten or partially molten debris was settled into a ring around Iapetus. Second, orbital decay drove the material towards the surface in the equatorial region. Third, the residual ring system gradually disappeared as the material deorbited and built up the ridge.

An ancient ring system should produce a ridge that is only slightly (by a matter of centuries or millennia) younger in age; however, the enhanced impactor population may also make the ridge more cratered and thus appear older. The low speed, shallow impacts from this model could also produce ragged craters preferentially elongated in the E-W direction, as was demonstrated in hydrocode simulations of a collapsing debris disk encircling Iapetus (Stickle and Roberts, 2017).

2.1.7. Impact generated

Three groups favored the hypothesis of impact-generated debris that subsequently built the equatorial ridge (Levison et al., 2011; Dombard et al., 2010, 2012; Kuchta et al., 2015). In this scenario, a large impact put material into orbit, after which the three groups diverge. Levison et al. (2011) proposed the impact put debris into orbit, forming a ring inside the Roche limit (the zone around a planetary body in which tidal forces would tear apart an orbiting body held together by gravity) and a fairly large sub-satellite outside. The sub-satellite pushed the ring material down on the surface, thus forming the ridge, and then the sub-satellite tidally evolved and helped despin Iapetus, eventually having its orbit destabilized and likely impacting Iapetus forming a large basin.

Alternatively, Dombard et al. (2010, 2012) proposed impact formation of a sub-satellite, the orbit of which decayed over larger time scales (potentially 1 Gyr) due to tides raised by Iapetus, eventually being torn apart within the Roche limit by tidal forces into a debris ring. This delay in ridge formation would increase the likelihood of preservation against the high-impact flux early in the solar system's history and allow ridge formation on a lithosphere that supports the ridge without apparent flexure.

Numerical modeling performed by Kuchta et al. (2015) indicated that tidal despinning alone is not sufficient to produce an equatorial ridge in addition to the synchronous rotation. By coupling tidal despinning and an abrupt change of rotation due to a giant impact, the initial model results suggested that it is possible to explain Iapetus's current rotation rate and equatorial ridge. The ejecta, produced by an impactor that is ~240–300 km in radius, would escape with some returning to the surface under Iapetus's gravity; however, the authors were unable to provide specific details or timing of the deformation process and impact event.

Notably, the three impact models and the ring model of Ip (2006) form the ridge in the same way: deorbiting of ring material over the equator via low-speed impacts at shallow angles. The exogenic models that involve a giant impact should produce a ridge that is younger in age, although the first (Levison et al., 2011) would, like the Ip model, only be centuries to millennia younger while the remaining could conceivably be hundreds of millions to a billion years younger, depending on the despinning time scale of Iapetus (e.g., Dombard et al., 2012). Also like the Ip model, the enhanced impactor population may make the ridge appear older. The low speed, shallow impacts from these models could also produce ragged craters preferentially elongated in the E-W direction.

2.2. Crater identification

Crater identification is performed using two simple cylindrical global mosaics of Iapetus: one generated primarily from Cassini data with some Voyager data filling the gaps (Roatsch et al., 2006), and the second composed solely of Cassini data that contains more high-resolution imagery (courtesy of P.M. Schenk). The mosaic generated by P.M. Schenk is 400 m/pxl with a superposed subregion of higher resolution imagery (pixel scale <100 m/pxl). In this study, the mosaic generated by P.M. Schenk is primarily used to locate all visible craters directly on and adjacent to the ridge. In instances where complete rims were unidentifiable, the mosaic generated by Roatsch et al. at a similar pixel scale is used for additional identification. For this study, we have chosen a conservative completeness value based on the resolution of the imagery used in this study (crater diameter $D = 10$ pxl; ~1 km for the high resolution imagery and 4 km for the global mosaic). It should be noted that the terrains and available imagery make crater identification more difficult than usual, and it is possible that the completeness value is larger than 10 pxl used here. Further, we removed data below this completeness limit so that the roll-off found in the relative size-frequency distribution plots (see Section 2.3) that is potentially due to the nature of the impactor population is not confused with the lack of recognition of small craters.

Using ArcGIS, crater identification and measurements are accomplished using the Crater Helper Tools v1.1 add-on for ArcMap 10 (Nava and Hare, 2011). Latitude and longitude recorded for each crater is the crater's approximate center as designated by the creation of an ellipse using the 6-point Ellipse tool. In addition, the lengths of the major and minor axes and their azimuths (measured clockwise from north) for the craters are recorded.

Before the craters are identified, the mosaics are visually inspected for regions with suitable conditions for crater recognition (e.g., sufficient image resolution, limited inaccuracies in overlapping images) and similar inherent and observational properties (e.g., incident angles, emission angles, pixel scales, and albedo). These regions are marked out and divided into preliminary study areas and are here after referred to as terrains (i.e., High Resolution Region, Leading Hemisphere, and Trailing Hemisphere). The final versions of the terrains (Fig. 1) are: Leading Hemisphere (LH), Leading Hemisphere Subregion (LHS), High Resolution Region (HRR), and Trailing Hemisphere (TH). The added subregion focuses on the crater population in a continuous region on the Leading Hemisphere that falls both on and off ridge. The total number of craters in the Leading Hemisphere thus includes the craters in the High Resolution Region and the Leading Hemisphere Subregion.

In order to study the difference in the cratering between on ridge and off ridge, all craters counted within 8° North and South latitude are considered "on ridge" based on a ridge that spans roughly 200 km wide (Dombard et al., 2012). Although the ridge is not continuous, the process that created the ridge had the potential to affect a zone of the same width. Once the terrains are finalized, the craters are subdivided into various latitude bands (on ridge −8° to 8° latitude; central ridge −4° to 4°; peripheral ridge −8° to −4° and 4° to 8°; and off ridge −40° to −8° and 8° to 40°) with their respective surface areas recorded for the statistical analysis portion of this study.

It was necessary to employ a method of identifying craters in areas of low resolution and non-optimal lighting. The resolution of the HHR at the equator can be as good as 9.8 m/pxl but areas outside this region have a significant drop in resolution and this increases the difficulty of the identification process. In regions of low resolution and poor lighting, crater rims are often unidentifiable. In most cases, the crater rims in the high resolution images are indicated by bright pixels (see Fig. 2). Crater rims in low resolution regions are identified by using the brightest pixels surrounding depressions (i.e., a central region of dark pixels). The observing and sunlight angles also have a major influence on determining the crater rim locations.

While a detailed morphological crater database is useful, further crater classification (e.g., simple, complex, and multi-ring

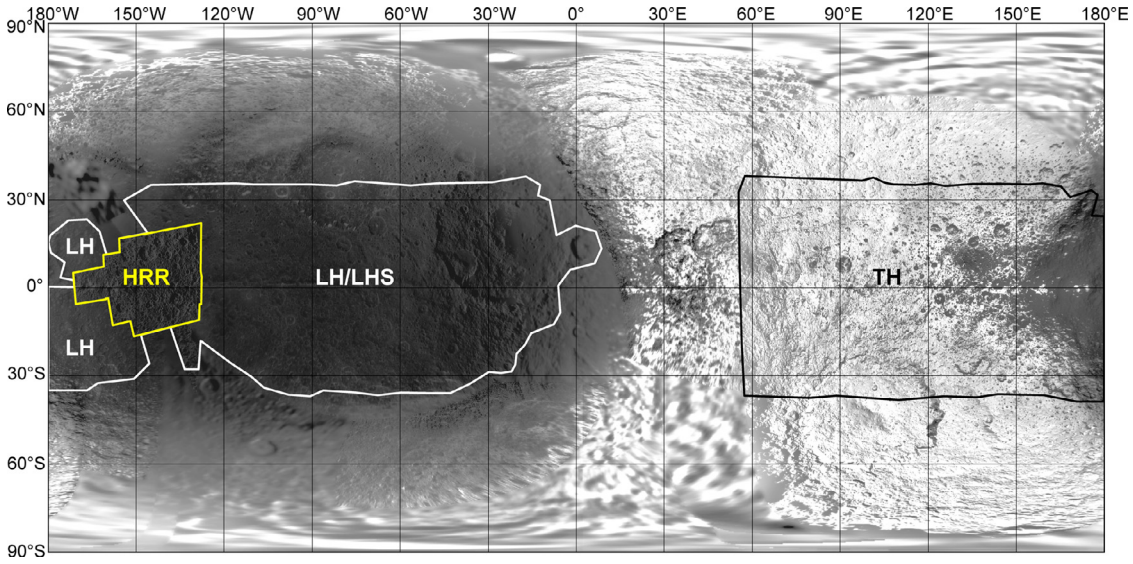

Fig. 1. Final terrain units determined for Iapetus – Leading Hemisphere (LH), Leading Hemisphere Subregion (LHS), High Resolution Region (HRR), and Trailing Hemisphere (TH).

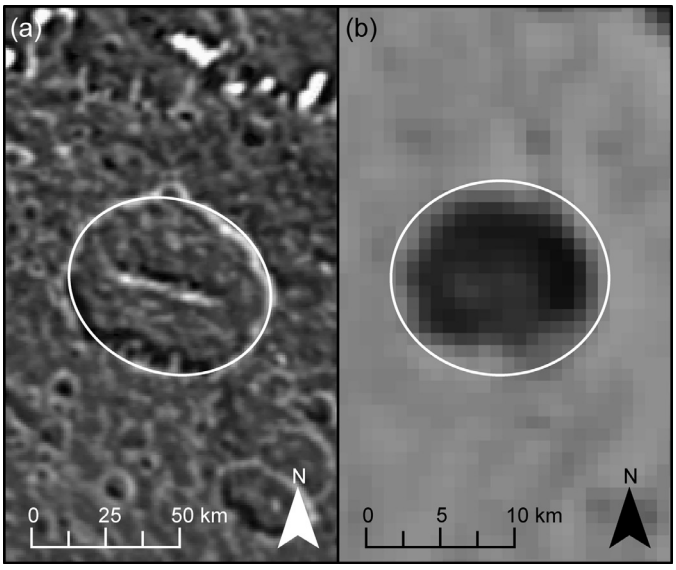

Fig. 2. Example of crater rims in (a) high resolution and (b) low resolution regions. The brightest pixels surrounding depressions (i.e., a central region of dark pixels) are used to mark crater rims in low resolution regions.

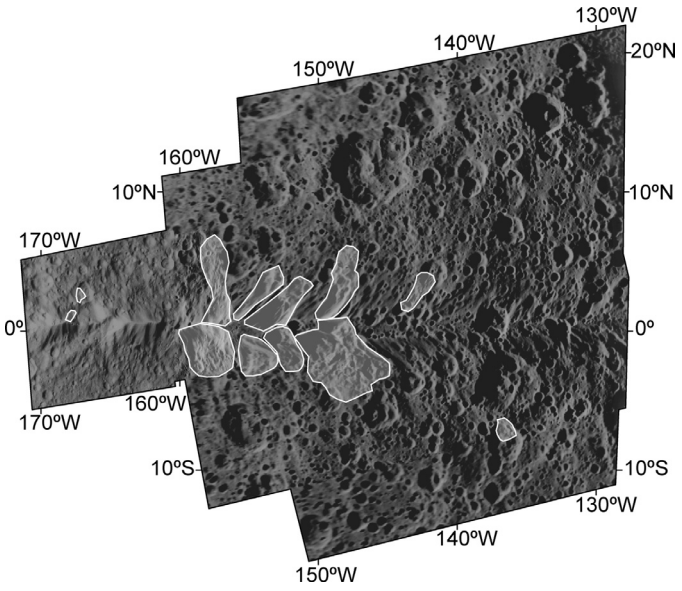

Fig. 3. Craters within the boundaries of mapped landsides were excluded from the database. Landslides have the potential to reduce the overall crater density and derivation of relative surface ages by effectively resetting the surface.

basin, ejecta deposits, etc.) is beyond the scope of this study. The presence of secondary craters is also known to complicate the use of crater densities to determine relative ages (e.g., McEwen and Bierhaus, 2006). However because of lower average impact speeds at Iapetus, the secondary crater population is expected to be negligible (Bierhaus et al., 2012). We did not identify any craters with obvious signs of secondary cratering (e.g., distinct clustering and chains).

The high relief of the equatorial ridge and presence of long-runout landslides on Iapetus plausibly hinder relative age calculations. Landslides have the potential to reduce the overall crater density and derivation of relative surface ages by effectively resetting the surface. A study by Singer et al. (2012) identified 12 large-scale landslides (up to 80 km in length) in the High Resolution Region (Fig. 3, landslide data courtesy of K. Singer). In this study, the craters that fall within the boundaries of the landslides are excluded from the database, and the mapped landslides are removed from the surface area to prevent overestimation of surface area when computing crater population statistics. Furthermore, it is unknown how well craters are retained on the slopes of the ridge; however, we expect this effect to be minimal.

2.3. Statistical analysis

Crater population statistics assist in the determination of planetary chronologies, dating geologic units, and identifying surface and subsurface processes. Our ultimate goal is to determine the relative differences in cratering between on ridge and off ridge. Size-frequency distributions are commonly used to determine relative surface ages.

We present the results of our crater counts in relative size-frequency distribution plot (R-plot) format (Crater Analysis Techniques Working Group, 1979). The relative age for surfaces of dif-

ferent ages will be indicated by the vertical displacement of plotted size-frequency distributions, with older surfaces higher on the plot. The shape of the curves can also provide insights into processes affecting the surface, such as crater saturation. Crater saturation plays a major role in this study and adds to the difficulty in assessing the relative ages of surfaces. Once saturation is reached, the crater density becomes constant and differences in relative age can be obscured. If the ridge has reached saturation, then it could be as heavily cratered as any other saturated surface. Saturation likely occurs around R values of 0.1–0.3 (Richardson, 2009) or about 2–10% geometric saturation (Gault, 1970). In this study, we plot this range of values (R = 0.1–0.3) to illustrate the potential value at which saturation could occur. Saturation is evaluated for craters at the assigned small and large crater bins: S ≤ 16 km and L > 16 km, where the size boundary is defined by an abrupt transition seen in the R-plots of the on-ridge craters (see below).

In this study, we also make use of rose diagrams to infer major axis orientation. Rose diagrams are utilized to infer crater orientation on ridge (−8° to 8° latitude) and off ridge (−40° to −8° and 8° to 40° latitude) at different diameter ranges (D > 8 km, 8 km ≤ D < 16 km, D ≥ 16 km). The craters are first sorted by absolute latitude and separated into three bins: central ridge (−4° to 4°), peripheral ridge −8° to −4° and 4° to 8°), and off ridge (40° to −8° and 8° to 40°). For each bin, the total number of craters is recorded for the major axis azimuth of 0–180°

3. Results

3.1. Database

Our crater database for Iapetus ranges from ±40° latitude and 0–360° longitude and contains 7748 craters ranging from 0.83 to 591 km in diameter (see Supplemental Database). Each entry in the database includes the terrain in which the crater is located, the center latitude and longitude of the crater, the major and minor axis length, and the azimuthal angle of orientation of the major axis. The four terrain units, shown in Fig. 1, contain varying degrees of crater densities. The total crater counts for the Leading Hemisphere and Trailing Hemisphere are 4504 and 3244, respectively.

3.2. Size-frequency distribution results

The results for the relative size-frequency distributions (R-plots) are presented in Figs. 4-5, and cumulative crater densities are given in Table 2. For the complete R-plots for all terrains, see Supplemental Figs. S1–S4. Fig. 4 shows the total crater population for the different regions and indicates that all terrain units on Iapetus reach or hover just below saturation at major-axis diameters D > 10 km, within uncertainty. It should be noted that the saturation levels may be higher for some regions given the practicalities of the subjective nature of identifying craters and the limited resolution of available imagery. For instance, the High Resolution Region tends to plateau at higher R-values than the other regions.

Fig. 5 provides a detailed comparison of on ridge and off ridge (Fig. 5a, c, e, and g) and a comparison of central ridge, peripheral ridge, and off ridge (Fig. 5b, d, f, and h). For the Leading Hemisphere and High Resolution Region, on ridge displays a substantial enhancement (> 3.0 sigma for the Poisson uncertainties used in this study) in small craters (D ≤ 16 km) compared to off ridge. The differences between on ridge and off ridge are less conclusive for craters larger than 16 km, which we attribute to fewer crater measurements and larger uncertainty. Another notable feature seen often in Fig. 5 (though most clearly in Fig. 5f) is the abrupt, systematic decrease in crater frequency between the ~16 and 20 km size bins. Small craters (D ≤ 16 km) appear saturated, but then suddenly drop in frequency for larger sizes, with perhaps a trend back towards saturation at the largest sizes. This abrupt transition between the ~16 and 20 km bins is difficult to reconcile with a continuous impactor population. The results for the Trailing Hemisphere also indicate that on ridge is under populated in small size craters; however, these results may be affected by observational biases introduced by poor image quality common for this hemisphere.

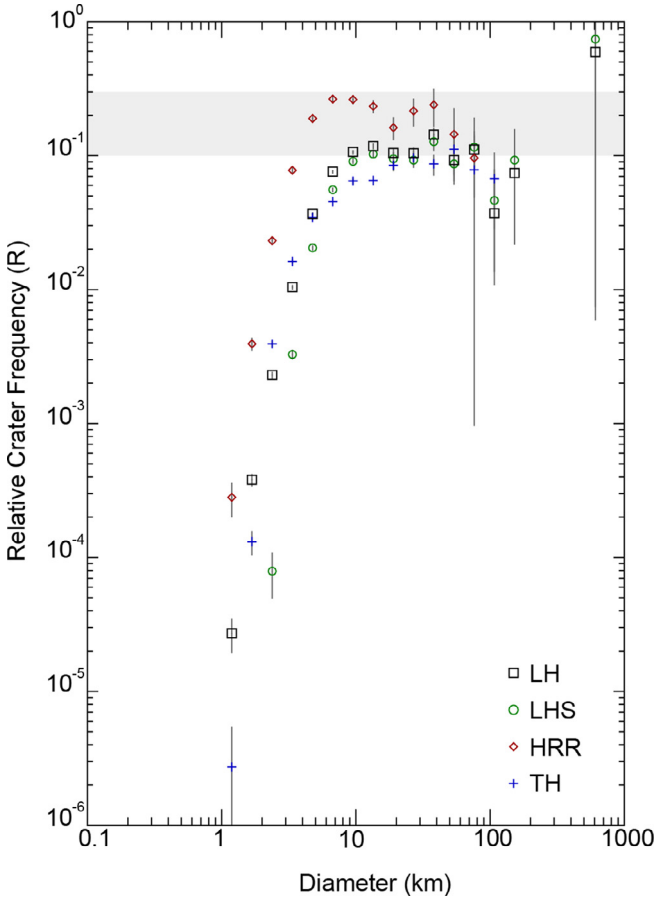

Fig. 4. Relative (R) size-frequency distributions of all terrain units on Iapetus. Diameters are binned by ($2^{0.5}$)D with one sigma Poisson bars. Modeled crater saturation is represented by the gray bar (R = 0.1–0.3). All terrain units likely reach or hover just below saturation at D > 10 km, within error.

3.3. Rose diagrams

Fig. 6 depicts the orientation results for the latitude bands in the High Resolution Region at different diameter ranges (D > 8 km, 8 km ≤ D < 16 km, D ≥ 16 km). The rose diagrams for the Leading Hemisphere, Leading Hemisphere Subregion, and Trailing Hemisphere are given in Supplemental Figs. S5–S7. The rose diagrams show the frequency at which the azimuthal angle of the major axis is measured clockwise from north. For each terrain unit, the complete crater database is sorted by latitude and separated into three bins: central ridge (−4° to 4°), peripheral ridge (−8° to −4° and 4° to 8°), and off ridge (−40° to −8° and 8° to 40°). The distribution of the terrain units with the highest resolution imagery (Fig. 6) and coarse resolution imagery (Supplemental Figs. S5–S7) shows no indication of an E-W orientation preference for any latitude bands.

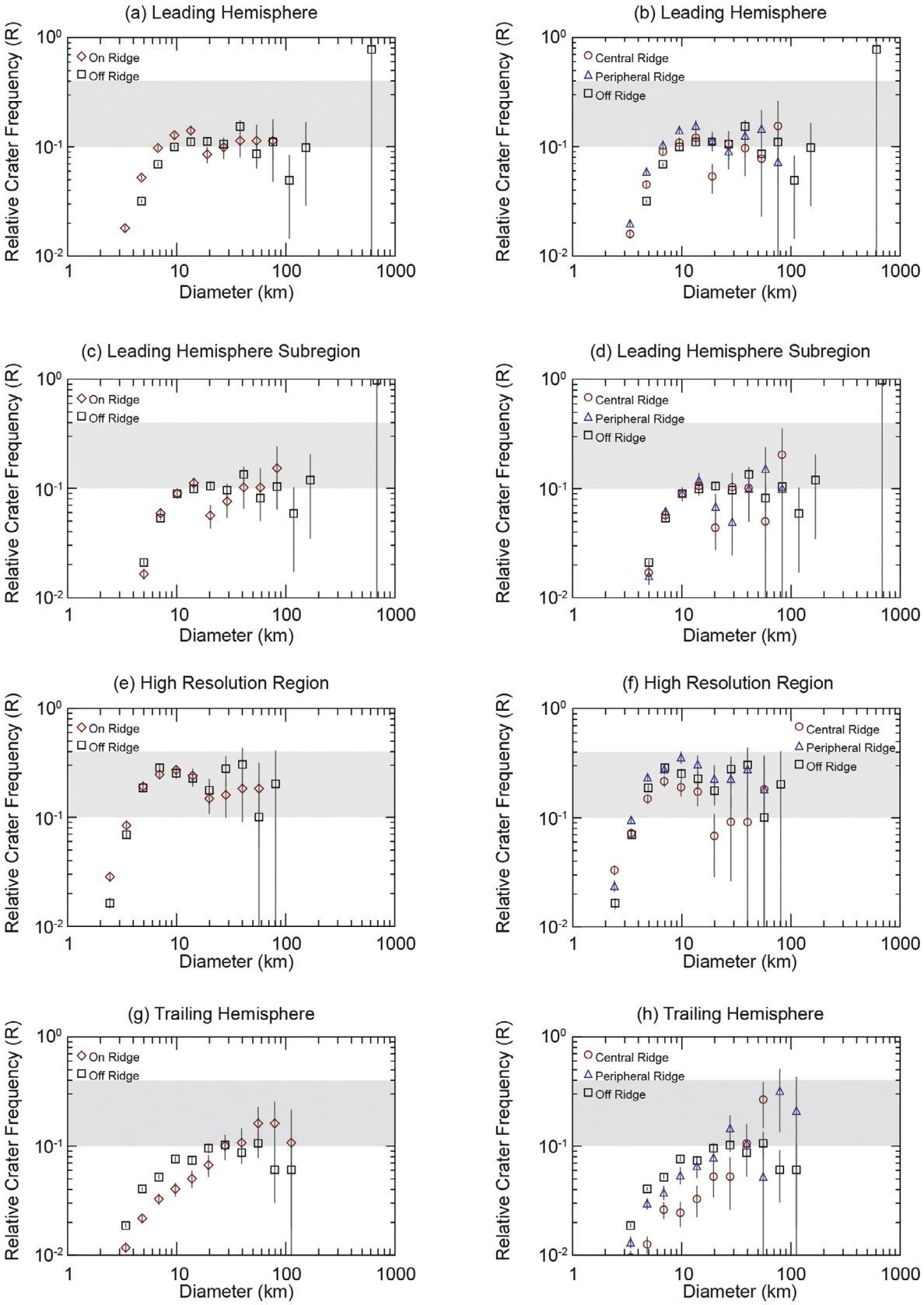

Fig. 5. Relative (R) size-frequency distributions of the Leading Hemisphere, Leading Hemisphere Subregion, High Resolution Region, and Trailing Hemisphere. Diameters are binned by $(2^{0.5})$D with one sigma error bars. Modeled crater saturation is represented by the gray bar (R = 0.1–0.3).

Table 2
Cumulative craters density for all terrain units on Iapetus.

Region	Terrain	Diameter	Crater Density[a]	Region	Terrain	Diameter	Crater Density[a]
LH	Whole Terrain	4–8	1151 ± 25	LHS	Whole Terrain	4–8	748 ± 23
		8–16	637 ± 19			8–16	548 ± 20
		16–32	151 ± 9			16–32	136 ± 10
	On Ridge	4–8	1550 ± 59		On Ridge	4–8	723 ± 47
		8–16	758 ± 41			8–16	567 ± 42
		16–32	129 ± 17			16–32	92 ± 17
	Central Ridge	4–8	1393 ± 81		Central Ridge	4–8	725 ± 67
		8–16	655 ± 55			8–16	551 ± 58
		16–32	103 ± 22			16–32	93 ± 24
	Peripheral Ridge	4–8	1697 ± 86		Peripheral Ridge	4–8	722 ± 66
		8–16	855 ± 61			8–16	582 ± 59
		16–32	153 ± 26			16–32	91 ± 23
	Off Ridge	4–8	1021 ± 27		Off Ridge	4–8	1248 ± 34
		8–16	598 ± 21			8–16	730 ± 26
		16–32	158 ± 11			16–32	193 ± 13
HRR	Whole Terrain	1-2	573 ± 58	TH	Whole Terrain	4–8	881 ± 24
		2–4	3811 ± 149			8–16	375 ± 16
		4–8	4981 ± 170			16–32	128 ± 9
		8–16	1465 ± 92				
		16–32	261 ± 39				
	On Ridge	1-2	916 ± 101		On Ridge	4–8	556 ± 41
		2–4	4381 ± 220			8–16	238 ± 27
		4–8	4856 ± 232			16–32	107 ± 18
		8–16	1512 ± 129				
		16–32	221 ± 49				
	Central Ridge	1-2	1193 ± 162		Central Ridge	4–8	385 ± 48
		2–4	4331 ± 309			8–16	153 ± 31
		4–8	3977 ± 296			16–32	73 ± 21
		8–16	1061 ± 153				
		16–32	110 ± 49				
	Peripheral Ridge	1-2	639 ± 119		Peripheral Ridge	4–8	727 ± 67
		2–4	4432 ± 313			8–16	324 ± 44
		4–8	5733 ± 356			16–32	141 ± 29
		8–16	1963 ± 208				
		16–32	331 ± 85				
	Off Ridge	1-2	195 ± 49		Off Ridge	4–8	973 ± 29
		2–4	3180 ± 197			8–16	413 ± 19
		4–8	5118 ± 250			16–32	134 ± 11
		8–16	1414 ± 131				
		16–32	305 ± 61				

[a] Cumulative crater density (in units per 10^6 km^2) for D≥ given with 1-sigma uncertainty

Table 3
Summarized results.

Terrain		Saturation[a]		Modified Craters	E-W Orientation		
		S	L		D < 8 km	8 km ≤ D < 16 km	D ≥ 16 km
LH	Whole Terrain	No	Yes	No	No	No	No
	On Ridge	No	No	No	No	No	No
	Central Ridge	No	No	No	No	No	No
	Peripheral Ridge	No	No	No	No	No	No
	Off Ridge	No	Yes	No	No	No	No
LHS	Whole Terrain	No	No	No	No	No	No
	On Ridge	No	No	No	No	No	No
	Central Ridge	No	No	No	No	No	No
	Peripheral Ridge	No	No	No	No	No	No
	Off Ridge	No	Yes	No	No	No	No
HRR	Whole Terrain	Yes	Yes	No	No	No	No
	On Ridge	Yes	No	No	No	No	No
	Central Ridge	Yes	No	No	No	No	No
	Peripheral Ridge	Yes	Yes	No	No	No	No
	Off Ridge	Yes	Yes	No	No	No	No
TH	Whole Terrain	No	No	No	No	No	No
	On Ridge	No	No	No	No	No	No
	Central Ridge	No	Yes	No	No	No	No
	Peripheral Ridge	No	Yes	No	No	No	No
	Off Ridge	No	No	No	No	No	No

[a] Based on R-plot – saturation at Small (S) and/or Large (L) crater bins: S ≤ 16 km and L > 16 km

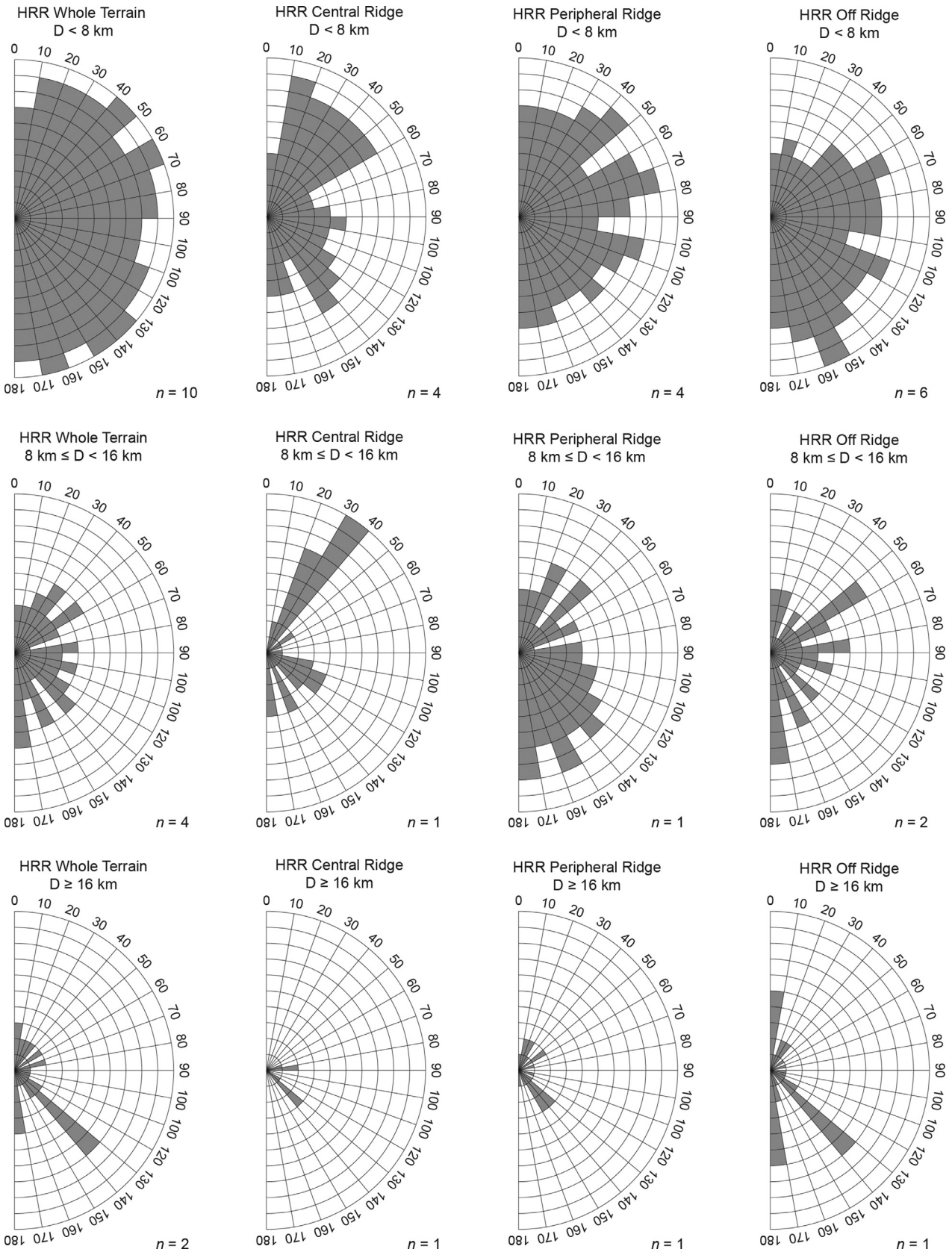

Fig. 6. Major axis rose diagrams for the High Resolution Region. The major axis of each crater is measured clockwise from north. Each diagram is binned in 10° increments ranging from 0° to 180°. The total number of craters in each individual cell is equal to *n*.

4. Discussion

Table 3 shows the summarized results for this study. The original hypothesis matrix (Table 1) includes Modified Craters as a possible identifier in the crater population. Visual inspection of the craters revealed no evidence of tectonic, volcanic, or surface resetting beyond crater saturation or landslides. Discussed below are the implications for each ridge formation hypotheses in combination with the summarized results.

In regions with the most fidelity (i.e., the High Resolution Region), the size frequency distributions show that on the ridge, there is a decrease in larger craters ($D > 16$ km) with a rather abrupt enhancement in smaller sizes ($D < 16$ km). In general, the ridge may be systematically depleted in larger craters for most terrains, though the uncertainties and possible saturation render this conclusion equivocal. If this observation is real and not due to other factors (e.g., observational biases), this abrupt change at ~16 km is difficult to reconcile with continuous crater populations. Observed crater populations of any common size-frequency distribution slope typically fall away from saturation at smaller craters gradually, not abruptly (Hartmann, 1984; Chapman and McKinnon, 1986). One possible interpretation of the data is that the ridge is a relatively younger surface with an enhanced small impactor population from a non-heliocentric source, thus allowing large craters to sit below saturation but with an abrupt transition to saturation at small sizes. The only current model that produces conditions with an enhanced small, non-heliocentric impactor population and depleted in larger craters preferentially along the ridge is the exogenic, impact generated sub-satellite model by Dombard et al. (2012). Here, the ridge can be much younger, explaining the lower degree of cratering at mid to large sizes, while the enhanced impactor flux arising from very comminuted, collisionally evolved debris from a tidally disrupted sub-satellite would explain the abrupt enhancement of small craters on the ridge.

Placing a younger age on the ridge would rule out all current endogenic ridge formation models, as the endogenic ridge formation models place the age of the ridge early on in Iapetus's history. In addition, most endogenic models would result in some form of crater transformation, which we defined by any crater subsequently overprinted by geologic processes. No evidence of modified craters is found in the crater population. Even if geologic processes, such as tectonics and volcanism did occur, there would be preferential removal of smaller craters, not larger ones.

With the exception the Dombard et al. (2012) model, the current exogenic models, primordial ring system (Ip, 2006) and impact generated ring system (Levison et al., 2011; Kuchta et al., 2015), also place the age of the ridge early on in Iapetus's history. An ancient ring system should produce a ridge that is only slightly (by a matter of centuries or millennia) younger in age; however, the expected enhanced impactor population may make the ridge more cratered and thus appear older. Both exogenic models that involve a giant impact should produce a ridge that is younger in age, although the ridge in the Levinson model would, like in the Ip model, only be centuries to millennia younger while in the Dombard model, it could conceivably being hundreds of millions to a billion years younger, depending on the despinning time scale of Iapetus.

Furthermore, the low speed, shallow impacts from the exogenic models might produce ragged craters preferentially elongated in the E-W direction along the equator. The rose diagrams did not indicate that the surface of Iapetus displays a preference for craters oriented in the E-W direction. However, one noticeable feature in the rose diagrams concerns craters on the ridge, which tend to be oriented obliquely between N-S and E-W. This concentration at oblique angles, however, is likely due to observational bias. The ridge is a three-dimensional structure viewed obliquely, the images from which are map projected in the basemaps. As a consequence, angles are affected. As evidence, the landslides shown in Fig. 3 should run N-S, but do not in the basemaps. Thus, the orientation of the long axes of the craters likely does not display a robust signal associated with the ridge and the orientation data cannot be used to discern any particular model.

The issue of crater saturation has been discussed in the literature extensively (e.g., Gault, 1970; Hartmann, 1984; Melosh, 1989; Richardson, 2009). The spatial density of impact craters reaches saturation equilibrium conditions with older terrains first and is reflected in crater counts that level off as a function of time and further bombardment. If crater saturation has not been reached for a particular crater diameter, then counting larger craters can form the basis for an estimate of the age of the surface. Fig. 4 indicates that all terrain units on Iapetus likely reach or hover just below saturation at $D > 10$ km, within error. In regions with the most fidelity (i.e., High Resolution Region and Leading Hemisphere), the R-plots show a slight decrease in larger sized craters with an increase in smaller sizes up to saturation on the ridge, while the rest of the off-ridge surface is likely sitting at saturation. This issue of saturation coupled with the relatively large errors on the counts, however, limits the robustness of any conclusions drawn from this study.

5. Conclusions

Iapetus is the only known body in the Solar System that has a mountainous equatorial ridge, and the formation of this feature is likely attributed to a key event in the evolution of the satellite. Various models have been proposed as the source of the ridge, all of which include predictions about the expected crater population. The objectives of this study have been to compile a database of the crater population on and around the equatorial ridge, to assess the relative age from differences in cratering between on ridge and off ridge, and to test the various models of ridge formation.

The size-frequency distributions of the craters are used to estimate relative terrain ages, interpret impactor population source, identify resurfacing events, and assess whether saturation has been reached. In regions with the most fidelity, the results may show a depletion of larger craters on the ridge with an enhancement in smaller sizes up to saturation. While the ridge does appear less cratered at larger sizes, the potential for surface resetting (i.e., via landslides) within close proximity to the ridge and the combination of large uncertainties and crater counts near saturation render these conclusions equivocal. Analysis of crater orientation reveal that overall, there is no preference for crater major-axis orientation.

Based on the results from the statistical analysis, it is concluded that the exogenic impact generated ridge formation model proposed by Dombard et al. (2012) is the most consistent with the observed crater population in this study, as it is the only current model that produces conditions with an enhanced small, non-heliocentric impactor population, yet can result in the ridge under populated in larger craters relative to off ridge (and hence be younger). While this study provides a broad overview of the craters on Iapetus, higher resolution imagery and further analysis of the crater population, such as morphologic classification, are needed to state definitively which ridge formation mechanism is most viable.

Acknowledgements

Support for this research was provided a graduate fellowship to A.L. Damptz by the Illinois Space Grant Consortium. The authors thank Dr. Paul Schenk for providing the global mosaic of Iapetus and Dr. Kelsi Singer for providing the landslide data. We also wish

to thank Dr. Stuart Robbins and Dr. Caleb Fassett for their constructive comments that improved this manuscript.

Supplementary materials

Supplementary material associated with this article can be found, in the online version, at doi:10.1016/j.icarus.2017.10.049.

References

Beuthe, M., 2010. East-west faults due to planetary contraction. Icarus 209, 795–817.

Bierhaus, E.B., Dones, L., Alvarellos, J.L., Zahnle, K., 2012. The role of ejecta in the small crater population on the mid-sized Saturnian satellites. Icarus, 218 602–621.

Castillo-Rogez, J.C., Matson, D.L., Sotin, C., Johnson, T.V., Lunine, J.I., Thomas, P.C., 2007. Iapetus' geophysics: rotation rate, shape, and equatorial ridge. Icarus 190, 179–202.

Chapman, C.R., McKinnon, W.B., 1986. Cratering of planetary satellites. In: Burns, J.A., Matthews, M.S. (Eds.), Satellites. Univ of Arizona Press, Tuscon, AZ, pp. 492–580.

Crater Analysis Techniques Working Group, 1979. Standard techniques for presentation and analysis of crater size-frequency data. Icarus 37, 467–474.

Czechowski, L., Leliwa-Kopystyński, J., 2008. The Iapetus's ridge: possible explanations of its origin. Adv. Space Res. 42, 61–69.

Denk, T., Neukum, G., Roatsch, T., Porco, C.C., Burns, J.A., Galuba, G.G., Schmedemann, N., Helfenstein, P., Thomas, P.C., Wagner, R.J., West, R.A., 2010. Iapetus: unique surface properties and a global color dichotomy from Cassini imaging. Science 327, 435–439.

Dombard, A.J., Cheng, A.F., McKinnon, W.B., Kay, J.P., 2010. The weirdest topography in the outer solar system: the ridge on Iapetus and its possible formation via giant impact. AGU Fall Meeting Abstract P31D-01.

Dombard, A.J., Cheng, A.F., McKinnon, W.B., Kay, J.P., 2012. Delayed formation of the equatorial ridge on Iapetus from a subsatellite created in a giant impact. J. Geophys. Res. 117, E03002. doi:10.1029/2011JE004010.

Dombard, A.J., Patterson, G.W., Lederer, A.P., Prockter, LM., 2013. Flanking fractures and the formation of double ridges on Europa. Icarus 223, 74–81.

Gault, D.E., 1970. Saturation equilibrium conditions for impact cratering on the Lunar surface: criteria and implications. Radio Sci. 5 (2), 273–291. doi:10.1029/RS005i002p00273.

Giese, B., Denk, T., Neukum, G., Roatsch, T., Helfenstein, P., Thomas, P.C., Turtle, E.P., McEwen, A., Porco, C.C., 2008. The topography of Iapetus' leading side. Icarus 193, 359–371.

Hartmann, W.K., 1984. Does crater "saturation equilibrium" occur in the Solar System? Icarus 60, 56–74.

Hirata, N., 2016. Differential impact cratering of Saturn's satellites by heliocentric impactors. J. Geophys. Res. Planets 121. doi:10.1002/2015JE004940.

Ip, W.-H., 2006. On a ring origin of the equatorial ridge of Iapetus. Geophys. Res. Lett. 33, L16203. doi:10.1029/2005GL025386.

Kay, J.P., Dombard, A.J., 2011. Unstable deformation and the formation of the equatorial bulge of Iapetus. Lunar Planet. Sci. XLII Abstract 2441.

Kirchoff, M.R., Schenk, P., 2009. Crater modification and geologic activity in Enceladus' heavily cratered plains: evidence from the impact crater distribution. Icarus 202, 656–668.

Kirchoff, M.R., Schenk, P., 2010. Impact cratering records of the mid-sized, icy satellites. Icarus 206, 485–497.

Kreslavsky, M.A., Nimmo, F., 2010. Critical spin as a possible origin of the Iapetus ridge. Bull. Am. Astron. Soc. 42, 941.

Kuchta, M., Tobie, G., Miljković, K., Běhounková, M., Souček, O., Choblet, G., Čadek, O., 2015. Despinning and shape evolution of Saturn's moon Iapetus triggered by a giant impact. Icarus 252, 454–465.

Levison, H.F., Walsh, K.J., Barr, A.C., Dones, L., 2011. Ridge formation and de-spinning of Iapetus via an impact-generated satellite. Icarus 214, 773–778.

Lopez Garcia, E.J., Rivera-Valentin, E.G., Schenk, P.M., Hammond, N.P., Barr, A.C., 2014. Topographic constraints on the origin of the equatorial ridge on Iapetus. Icarus 237, 419–421.

Martin, E.S., Jurdy, D.M., 2010. Iapetus: construction and analysis of a global crater database. Lunar Planet. Sci. XLI Abstract 1437.

McEwen, A.S., Bierhaus, E.B., 2006. The importance of secondary cratering to age constraints on planetary surfaces. Annu. Rev. Earth Planet. Sci. 34, 535–567.

Melosh, H.J., 1977. Global tectonics of a despun planet. Icarus 31, 221–243.

Melosh, H.J., 1989. Impact Cratering: A Geologic Process. The Claredon Press, Oxford University Press, New York.

Melosh, H.J., Nimmo, F., 2009. An intrusive dike origin for Iapetus' enigmatic ridge? Lunar Planet. Sci. XL Abstract 2478.

Nava, R.A., and T.M. Hare (2011), A GIS toolset for the rapid measurement and cataloging of morphologic features in planetary mapping, Abstract. Available for download from the PIGWAD (http://webgis.wr.usgs.gov) and ESRI Resource Center (http://resources.arcgis.com/gallery/file/arcobjects-net-api/) websites.

Neukum, G., Wagner, R.J., Denk, T., Porco, C.C.the Cassini ISS Team, 2005. The cratering record of the Saturnian satellites Phoebe, Tethys, Dione and Iapetus in comparison: first results from analysis of the Cassini ISS imaging data. Lunar Planet. Sci. XXXVI Abstract 2034.

Peale, S.J., 1977. Rotation histories of the natural satellites. In: Planetary Satellites. Univ. of Ariz. Press, Tucson, pp. 87–112.

Pechmann, J.B., Melosh, H.J., 1979. Global fracture patterns of a despun planet: application to Mercury. Icarus 38, 243–250.

Porco, C.C., Baker, E., Barbara, J., Beurle, K., Brahic, A., Burns, J.A., Charnoz, S., Cooper, N., Dawson, D.D., Del Genio, A.D., Denk, T., Dones, L., Dyudina, U., Evans, M.W., Giese, B., Grazier, K., Helfenstein, P., Ingersoll, A.P., Jacobson, R.A., Johnson, T.V., McEwen, A., Murray, C.D., Neukum, G., Owen, W.M., Perry, J., Roatsch, T., Spitale, J., Squyres, S., Thomas, P.C., Tiscareno, M., Turtle, E., Vasavada, A.R., Veverka, J., Wagner, R., West, R., 2005. Cassini imaging science: Initial results on Phoebe and Iapetus. Science 307, 1237–1242.

Richardson, J.E., 2009. Cratering saturation and equilibrium: a new model looks at an old problem. Icarus 204, 697–715. doi:10.1016/j.icarus.2009.07.029.

Rivera-Valentin, E.G., Barr, A.C., Lopez Garcia, E.J., Kirchoff, M.R., Schenk, P.M., 2014. Constraints on planetesimal disk mass from the cratering record and equatorial ridge on Iapetus. Astrophys. J. 792 #127.

Roatsch, Th., Wahlisch, M., Scholten, F., Hoffmeister, A, Matz, K.-D., Denk, T., Neukum, G., Thomas, P., Helfenstein, P., Porco, C., 2006. Mapping of the icy Saturnian satellites: first results from Cassini-ISS. Planet. Space Sci. 54, 1137–1145.

Roberts, J.H., Nimmo, F., 2009. Tidal dissipation due to despinning and the equatorial ridge on Iapetus. Lunar Planet. Sci. XL Abstract 1927.

Robuchon, G., Choblet, G., Tobie, G., Čadek, O., Sotin, C., Grasset, O., 2010. Coupling of thermal evolution and despinning of early Iapetus. Icarus 207, 959–971.

Sandwell, D., Schubert, G., 2010. A contraction model for the flattening and equatorial ridge of Iapetus. Icarus 210, 817–822.

Schmedemann, N., Neukum, G., Denk, T., Wagner, R., 2008. Stratigraphy and surface ages on Iapetus and other Saturnian satellites. Lunar Planet. Sci. XXXIX Abstract 2070.

Schmedemann, N., Neukum, G., Denk, T., Wagner, R., 2009. Impact crater size-frequency distribution (SFD) on Saturnian satellites and comparison with other Solar-System bodies. Lunar Planet. Sci. XL Abstract 1941.

Singer, K.N., McKinnon, W.B., Schenk, P.M., Moore, J.M., 2009. Large landslides on Iapetus: implications for crater and ridge modification. Bull. Am. Astron. Soc. 41 Abstract 38.01.

Singer, K., McKinnon, W.B., 2011. Tectonics on Iapetus: despinning, respinning, or something completely different? Icarus 216, 198–211.

Singer, K.N., McKinnon, W.B., Schenk, P.M., Moore, J.M., 2012. Massive ice avalanches on Iapetus mobilized by friction reduction during flash heating. Nat. Geosci. 5, 574–578.

Stickle, A.M., Roberts, J.H., 2017. Building a ridge that Iapetus pays for. Lunar Planet. Sci. XLVIII Abstract 1262.

Thomas, P.C., Burns, J.A., Helfenstein, P., Squyres, S., Veverka, J., Porco, C., Turtle, E.P., McEwen, A., Denk, T., Giese, B., Roatsch, T., Johnson, T.V., Jacobson, R.A., 2007. Shapes of the Saturnian icy satellites and their significance. Icarus 190, 573–584.

Thomas, P.C., 2010. Sizes, shapes, and derived properties of the Saturnian satellites after the Cassini nominal mission. Icarus 208, 395–401.

Weidenschilling, S.J., 1981. How fast can an asteroid spin? Icarus 46, 124–126.